

## ABSTRACT

Improving the Quality of Proton CT Scan Images by Utilizing Straggling Power

Jordan Lee Reeser, M.S.E.C.E

Chairperson: K. Schubert, Ph.D.

Proton therapy has grown in interest within the medical community for its promise in cancer treatment. Proton CT (pCT) scans are an essential part of this process to map treatment areas, but a common problem is the lack of precision along the artifact boundaries within the image. It was hypothesized that combining two forms of collected data, stopping power and scattering power, may result in a sharper image. Initial testing harnessed typical filtering techniques to improve the combined image, but did not result in sharpened boundaries. Further testing harnessed knowledge of the data itself, such as respective contained information, and medical imaging techniques to improve the combined image. Qualitative analysis by inspection was verified quantitatively by calculating the FWHM. These results showed an average improvement of 0.3967 mm for the combined image compared to the stopping power image.

Improving the Quality of Proton CT Scan Images by Utilizing Straggling Power

by

Jordan Lee Reeser, B.S.E.C.E

A Thesis

Approved by the Department of Electrical and Computer Engineering

---

Kwang Y. Lee, Ph.D., Chairperson

Submitted to the Graduate Faculty of  
Baylor University in Partial Fulfillment of the  
Requirements for the Degree  
of  
Master of Science

Approved by the Thesis Committee

---

K. Schubert, Ph.D., Chairperson

---

S. Kim, Ph.D.

---

R. Marks, Ph.D.

---

L. Olafsen, Ph.D.

---

A. Spence, Ph.D.

Accepted by the Graduate School  
May 2021

---

J. Larry Lyon, Ph.D., Dean

Copyright © 2021 by Jordan Lee Reeser  
All rights reserved

## TABLE OF CONTENTS

LIST OF FIGURES .....	v
LIST OF ABBREVIATIONS.....	vii
ACKNOWLEDGMENTS .....	viii
CHAPTER ONE	
Introduction .....	1
<i>Bragg Curve</i> .....	2
<i>pCT Scan</i> .....	3
<i>Statistical Data</i> .....	4
<i>Motivation</i> .....	5
<i>Straggling Power</i> .....	5
<i>Methods</i> .....	6
<i>Contributions</i> .....	6
CHAPTER TWO	
Processing Combined Image Using Filtering Techniques .....	7
<i>Introduction</i> .....	7
<i>Background</i> .....	7
<i>Discussion</i> .....	18
CHAPTER THREE	
Applying Knowledge of Straggling Power Data to Adjust Image .....	19
<i>Introduction</i> .....	19
<i>Background</i> .....	20
<i>Procedure and Results</i> .....	20
<i>Quantitative Analysis</i> .....	31
<i>Discussion</i> .....	33
CHAPTER FOUR	
Conclusion .....	34
APPENDIX A	
Code Appendix.....	37
BIBLIOGRAPHY .....	41

## LIST OF FIGURES

Figure 1.1.	(a) Slice image from the Harvard Cyclotron proton CT scanner published in 2000 and (b) a slice image from a contemporary X-ray CT scanner. These images are rotated with respect to one another. The phantom diameter is 9.5 cm. ©Institute of Physics and Engineering in Medicine. Reproduced from Zygmanski <i>et al.</i> with permission from IOP Publishing. All rights reserved. ....	1
Figure 1.2.	Graph depicting the Bragg curves for a photon beam, modified proton beam, and a single proton beam. Image is reproduced with permission from Wikimedia Commons [1]. All rights reserved.	2
Figure 2.1.	Original phantom image, generated stopping power image, and generated straggling power image. ....	8
Figure 2.2.	Morphology open filter applied to a binary image. Image reproduced with permission. ©2003 R. Fisher, S. Perkins, A. Walker and E. Wolfart. All rights reserved. ....	10
Figure 2.3.	Original image (left) and image filtered with the tophat filter (right). Images reproduced with permission. ©1994-2021 The MathWorks, Inc. All rights reserved. ....	10
Figure 2.4.	Image of coins with salt and pepper noise (left) and median filtered image (right). Image reproduced with permission. ©1994-2021 The MathWorks, Inc. All rights reserved. ....	11
Figure 2.5.	Combined proton image produced by adding stopping power and straggling power images. ....	12
Figure 2.6.	Original stopping power image (left) and the image with open filter applied (right). ....	13
Figure 2.7.	Zoomed in interior section of the original stopping power image (left) and the zoomed in interior section of the image with open filter applied (right). ....	13
Figure 2.8.	Zoomed in exterior section of the original stopping power image (left) and the zoomed in exterior section of the image with open filter applied (right). ....	13
Figure 2.9.	Original straggling power image (left) and the image with tophat filter applied (right). ....	14

Figure 2.10. The new combined image with the filtered stopping and straggling power. ....	15
Figure 2.11. Combined image forcing pixels to be black where corresponding stopping power pixels are black. ....	16
Figure 2.12. Final combined image after application of open filter and median filter. ....	17
Figure 2.13. Final combined image (left) compared to the original stopping power image (right). ....	18
Figure 3.1. RSP vs. depth in cm line graphs of stopping power, straggling power, and combined with a straggling power weight of 1. ....	22
Figure 3.2. RSP vs. depth in cm line graphs of stopping power, straggling power, and combined with a straggling power weight of 0.4. ....	22
Figure 3.3. Position of data taken for line graphs on original phantom. ....	23
Figure 3.4. Generated phantom mask. ....	24
Figure 3.5. Straggling power with and without mask applied. ....	24
Figure 3.6. Line graph cross section with masked and weighted straggling power. ....	25
Figure 3.7. Zoomed in cross section of modified combined image. ....	26
Figure 3.8. Line graph cross section with masked and weighted straggling power for phantom size $16000 \times 16000$ bits and stopping/straggling sections of $50 \times 50$ bits. ....	27
Figure 3.9. Zoomed in cross section for phantom size $16000 \times 16000$ bits and stopping/straggling sections of $50 \times 50$ bits. ....	27
Figure 3.10. Line graph cross section with masked and weighted straggling power for phantom size $32000 \times 32000$ bits and stopping/straggling sections of $50 \times 50$ bits. ....	28
Figure 3.11. Zoomed in cross section for phantom size $32000 \times 32000$ bits and stopping/straggling sections of $50 \times 50$ bits. ....	29
Figure 3.12. Line graph cross section with masked and weighted straggling power for phantom size $64000 \times 64000$ bits and stopping/straggling sections of $200 \times 200$ bits. ....	30
Figure 3.13. Zoomed in cross section for phantom size $64000 \times 64000$ bits and stopping/straggling sections of $200 \times 200$ bits. ....	30

## LIST OF ABBREVIATIONS

MS	Master of Science
PhD	Doctor of Philosophy
CT	Computed Tomography
pCT	Proton Computed Tomography
MCS	Multiple Coulomb Scattering
MLP	Most Likely Path
CST	Cubic Spline Trajectory
FBP	Filtered Back Projection
ART	Algebraic Reconstruction Technique
FWHM	Full width at half maximum
RSP	Relative stopping power

## ACKNOWLEDGMENTS

I would like to thank all of the Engineering professors that I have had the opportunity to work with during my time at Baylor for their positive impact on my development as an engineer. I especially would like to thank Dr. Schubert for his mentorship during the past few years. His mentorship has helped me achieve success both academically and professionally.

## CHAPTER ONE

### Introduction

From as early as the 1960s, proton therapy has been suggested as a possible alternative to X-ray therapy for treatment of cancer [2, 3, 4]. Since then, significant progress has been made in the development of proton radiography and tomography, but several challenges still remain. Prior to treatment, a proton computed tomography (pCT) scan is conducted in order to outline structures and produce maps of electron density and nuclear interactions [2]. Recent experiments of pCT scanning show promise in producing a viable image, but there has been notable difficulty in producing sharp edges along the artifacts within the image [2, 5, 6, 7]. An example of this is shown in Figure 1.1 which depicts a phantom slice acquired by reconstructing a pCT scan using a 159-MeV proton beam at the Harvard Cyclotron alongside the same slice of an image reconstructed from an X-ray CT scan [2].

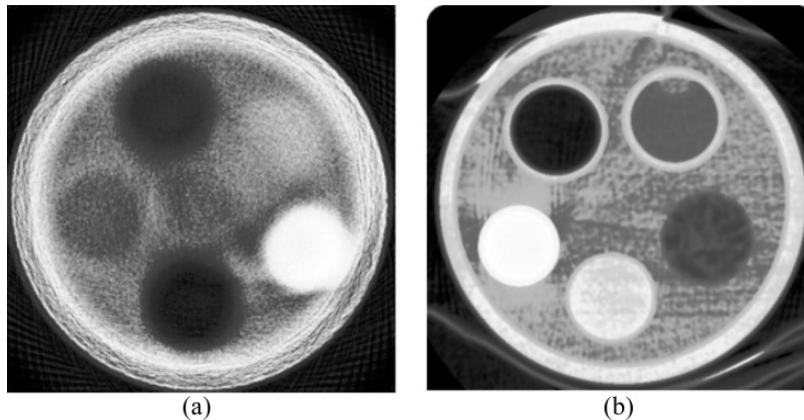


Figure 1.1: (a) Slice image from the Harvard Cyclotron proton CT scanner published in 2000 and (b) a slice image from a contemporary X-ray CT scanner. These images are rotated with respect to one another. The phantom diameter is 9.5 cm. ©Institute of Physics and Engineering in Medicine. Reproduced from Zyganski *et al.* with permission from IOP Publishing. All rights reserved.

Though pCT scan images have improved since this example from 2000, this image highlights how the pCT scan images do not have sharp edges in comparison to those generated by X-ray CT scans. It is proposed that incorporating additional data collected during the pCT scans will help improve the edge quality of artifacts, therefore improving the viability of pCT scans and proton therapy for use in medical treatment.

### *Bragg Curve*

Proton therapy is of interest in the medical community due to the nature of a proton beam's Bragg curve [3, 5, 8]. The Bragg curve plots loss of ionizing radiation while traveling through matter. For protons, the curve resembles that of  $e^x + n$  where  $n$  is the initial dose. This means that the Bragg peak occurs right before the proton loses energy [5, 8]. This effect is shown in Figure 1.2 which displays a graph comparing the Bragg curves of a single proton beam, a modified proton beam (multiple protons), and a photon (X-ray) beam.

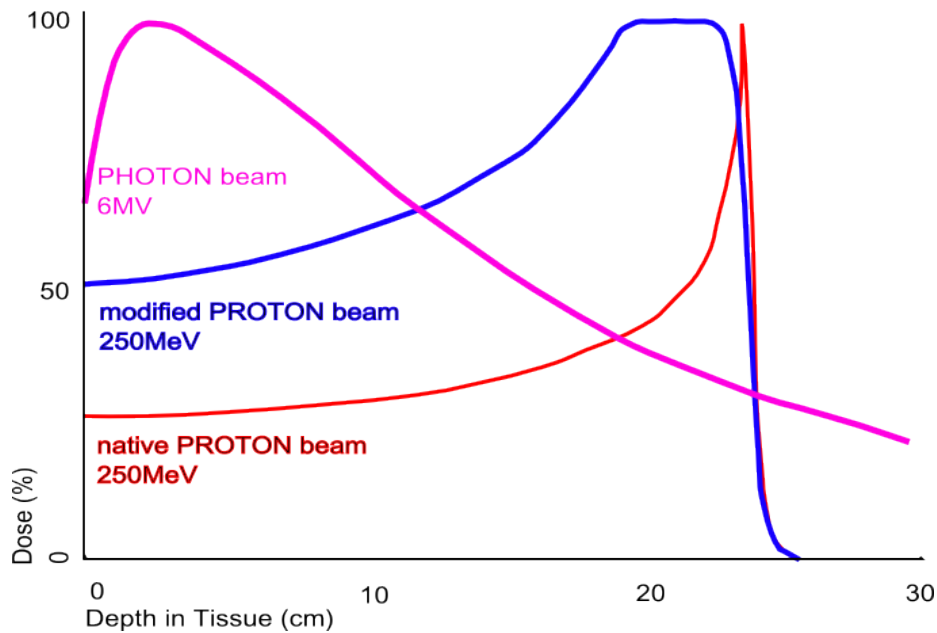


Figure 1.2: Graph depicting the Bragg curves for a photon beam, modified proton beam, and a single proton beam. Image is reproduced with permission from Wikimedia Commons [1]. All rights reserved.

The difference in the Bragg curve of the photon beam and the proton beam displays the potential that proton therapy has for cancer treatment. The location of the Bragg peak can be placed by adjusting the energy applied to the beam. This allows for more precision in targeting cancerous cells without irradiating healthy cells [3]. The Bragg curve of the X-ray, on the other hand, cannot be modified, so only a small amount of radiation may actually hit the target area while any other tissue along the path will be hit with nearly the same amount of radiation. The intensity of the proton beam Bragg peak requires precision while placing since any error could deposit the maximum dose of radiation at healthy tissue [8, 9, 10]. Thus, an accurate treatment map is of great importance.

### *pCT Scan*

A treatment map is usually developed by taking a CT scan or radiography of the area. The scan maps the electron density and nuclear interactions [11]. Initially, traditional X-ray CT scans were used for the treatment map, but since the interaction of protons in materials is different than that of photons, this strategy introduced extra error when determining how much energy to give the proton beam for the placement of the Bragg peak [11]. Proton CT scans were then introduced as an alternative that would more accurately approximate the proton interaction [5, 10, 12]. pCT scans are conducted similarly to that of traditional X-ray CT scans where a series of images are taken at different angles. A 2D cross-section of the scan is then reconstructed to form the image from the measured energy loss of the protons as they pass through the subject [6]. However, calculating the energy loss of the proton beam is a much more difficult process than that of X-ray CT scans since protons undergo multiple coulomb scattering (MCS). Protons interact and collide with other particles while traveling through a material, resulting in random deviations from the initial beam path. As the number of interactions becomes high, the angular dispersion of the proton beam

can be modeled as a Gaussian curve [13]. The proton scattering cannot be removed by devices such as collimators as it can for photons, but several different methods have been developed to account for the MCS effect; the two main approaches are the Most Likely Path (MLP) and Cubic Spline Trajectory (CST) [5]. The MLP method requires the entrance and exit positions and angles while CST requires entrance and exit position vectors and the direction vector [5, 8]. With this information, the image can be reconstructed with either Filtered Back Projection (FBP) or the Algebraic Reconstruction Technique (ART) [14].

### *Statistical Data*

Taking the pCT scan produces four different statistics:

- (1) Proton direction (scattering power)
- (2) Lateral position or energy spread (straggling power)
- (3) Energy loss (stopping power)
- (4) Stopping depth (fluence)

The scattering power is a product of the MCS effect; when protons undergo MCS, they experience random deviations in the path direction. Lateral deviations within in the scattering power produces the straggling power. Stopping power is caused by the excitation and ionization of atomic electrons, and fluence is predominantly caused by energy loss [2, 7]. Each of these statistics can be used to reconstruct an image, but some contain more useful information than others. Scattering and stopping power both contain the majority of the structural information, so are the most commonly used for pCT scanning [7]. Both of these statistics independently generate a decent quality image that has proper structural shape and brightness, however they lack precision along the boundaries of internal artifacts within the scan [7]. The straggling power contains the least amount of structural information, and thus has rarely been used to reconstruct an image.

### *Motivation*

The pCT treatment map is used to determine the depth of the target area within the patient in order to determine the amount of energy that should be applied to the proton beam in order to place the Bragg peak at the desired location [9]. When treating cancerous tumors, it is very important to destroy the entirety of the tumor in order to prevent it from growing, so it needs to be planned for the entire area to be hit with a proton Bragg peak [6, 15]. Due to the proton Bragg peak, proton treatment is more sensitive to errors than photon radiation. Even a small amount of error in the treatment map along internal structures such as tumors could cause the Bragg peak to be accidentally placed too shallow or too deep within the patient during treatment. This would result in either cancerous cells being missed and therefore allowing the tumor to regrow or in hitting healthy cells with a large amount of radiation [9]. pCT scans made by reconstructing only the scattering power or stopping power are known to have a lack of precision along internal artifact boundaries, which increases the likelihood of incorrectly placing the proton Bragg peak. It was hypothesized that incorporating the straggling power, which contains more edge data, along with the stopping power could result in sharper pCT edges.

### *Straggling Power*

As stated earlier, the straggling power statistic is the lateral deviations in the scattering power, or also known as the standard deviation of a Gaussian fit on the scattering power [16]. This data is typically regarded as error and removed [14]. When protons enter a uniform medium, they will tend to spread approximately uniformly in random directions. From a single beam, the radial spread will be determined by the density of the medium. If another medium is introduced and the proton beam is directed tangential to the boundary, fewer protons will spread into the more dense material, leaving more protons in the less dense material. The larger the difference in

density, the larger of a difference will be seen in the spread; this difference in proton spread is the straggling power. Reconstructed images of this statistic will show the boundaries where a change in material density occurs, and this effect will be larger where the density difference is greater.

### *Methods*

For the experiments discussed in this document, MATLAB is used as the primary environment and language. MATLAB contains extensive existing libraries for medical imaging simulation and image processing that are very useful for this application. For a proof of concept, simulated data is used. For a usual pCT scan, each data statistic is captured within the large amount of sinogram data. Since MATLAB does not have functions specifically to generate a simulated pCT scan, the simulated stopping power and straggling power need to be generated. This is done by producing a larger phantom image using MATLAB's phantom function, and then the sinogram is generated by taking the radon transform. To simulate the data collected by sensors, small sections of a determined size on each line of the sinogram are averaged to simulate the stopping power, and the standard deviation of the same sections are taken to simulate the straggling power.

### *Contributions*

The experiments discussed in this paper show a successful result in the combination of stopping power and straggling power to sharpen the edges of internal artifacts within a pCT scan. These results are verified by inspection and quantitatively by comparing the full width at half maximum (FWHM) for the different regions of the phantom cross section for the original image, stopping power image, and combined image. These results are verified for different image resolutions to show robustness for possible differences in pCT equipment.

## CHAPTER TWO

### Processing Combined Image Using Filtering Techniques

#### *Introduction*

Initial testing of the hypothesis that combining stopping power and straggling power would produce a sharper image was conducted using a small, computer generated phantom image of size  $4000 \times 4000$  bits. The stopping power image was then approximated by taking the mean of  $10 \times 10$  bit sections of the original phantom, and the straggling power image was approximated by taking the standard deviation of the same  $10 \times 10$  bit sections of the original phantom. Adding the stopping power and straggling power data provided the initial combined phantom image. This initial image displayed a substantial amount of constructive interference from the image reconstruction algorithm. To mitigate the additional error, the stopping power image was preprocessed with a morphology open filter, and the straggling power image was preprocessed with a morphology tophat filter. The combined image was then post-processed with a median filter and a morphology open filter. The implementation of these filters successfully removed much of the error induced by the image reconstruction algorithm, but blurred the edges of internal structures with lower contrast in brightness. Thus this technique was not beneficial for the task of sharpening the edges of artifacts within the phantom.

#### *Background*

##### *Phantoms*

The phantom images are generated using MATLAB's phantom command. For this study, Modified Shepp-Logan phantoms of size  $4000 \times 4000$  bits are used. These phantoms simulate a head scan with internal hematomas. Stopping power quantifies

the typical energy lost by a proton passing through a region, which in this case is a  $10 \times 10$  pixel region. The stopping power image is thus approximated by the mean of each group of 10 pixels (the detectors) on every line of the sinogram. This is a reasonable approximation of what is done in the actual medical device for each proton that has the same entry and exit values. Straggling power is the standard deviation on the detectors and is calculated by taking the standard deviation of each 10 pixel "detector" in the sinogram. This results in stopping power and straggling power images of size  $400 \times 400$  bits. Figure 2.1 shows the original phantom with generated stopping power and straggling power images.

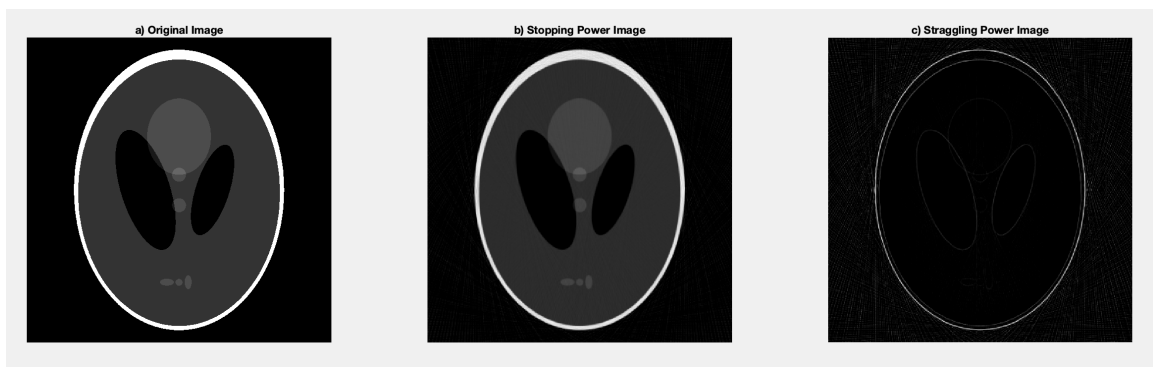


Figure 2.1: Original phantom image, generated stopping power image, and generated straggling power image.

### *Reconstruction Algorithm*

Filtered back projection (FBP) is used to reconstruct the images from their radon transforms. This reconstruction algorithm was chosen since it provides a high quality reconstruction in a short compute time. The projection data of the image is obtained by taking the radon transform  $g(s, \theta) = Rf$  where  $f$  is the image,  $R$  is the radon transform, and  $g(s, \theta)$  is the sinogram (projection) data. The radon transform takes the function  $f$  defined on a plane and transforms it to a function  $Rf$  defined on a 2D space of lines on that plane; the value at each line is equal to the line integral

of  $f$  along that line. Therefore, the reconstructed image can be found by solving the matrix equation  $f = R^{-1}g$  [14, 17]. The FBP algorithm accomplishes this by first taking the Fourier Transform of  $g$ , then applying the ramp filter ( $|\omega|$ ). The inverse Fourier Transform  $F^{-1}$  is then taken, resulting in FBP transformed sinogram data  $g_{filt}$  shown in Equation 2.1 [18, 19]:

$$g_{filt}(s, \theta) = F^{-1}(|\omega|F(g(s, \theta))) \quad (2.1)$$

$g_{filt}$  is then back projected (added to each pixel) along the lines perpendicular to the angled lines that compose the sinogram. This is then repeated for each line of the sinogram.

### *Filtering Techniques*

Several filtering techniques are used to remove error and clarify the images. The morphology open filter is used to preprocess the stopping power and as one of the post-processing filters in order to remove small streak artifacts. This filter performs erosion followed by dilation which has the effect of preserving black in the image while removing some white. This effect is shown on a binary image in Figure 2.2. It should be noted that the binary morphological effect can be replicated in greyscale by assigning minimum and maximum values within the neighborhood being processed [20].

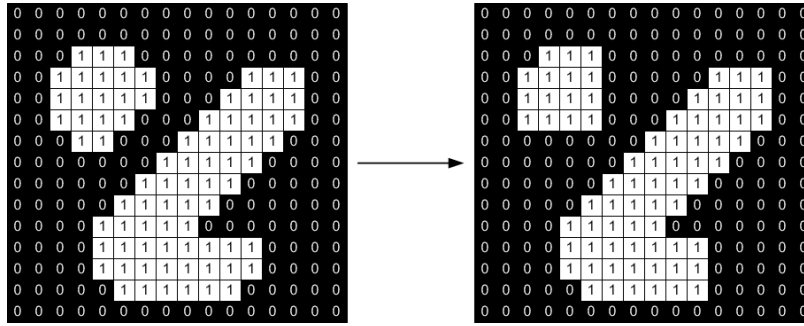


Figure 2.2: Morphology open filter applied to a binary image. Image reproduced with permission. ©2003 R. Fisher, S. Perkins, A. Walker and E. Wolfart. All rights reserved.

The morphology tophat filter is used to preprocess the straggling power data to remove random noise and large scale variations which often appear in the image while preserving the characteristically thin linear outlines of the edges in a straggling power image. The tophat filter first applies the morphology open filter, then subtracts the opened image from the original. This effect is shown in Figure 2.3.

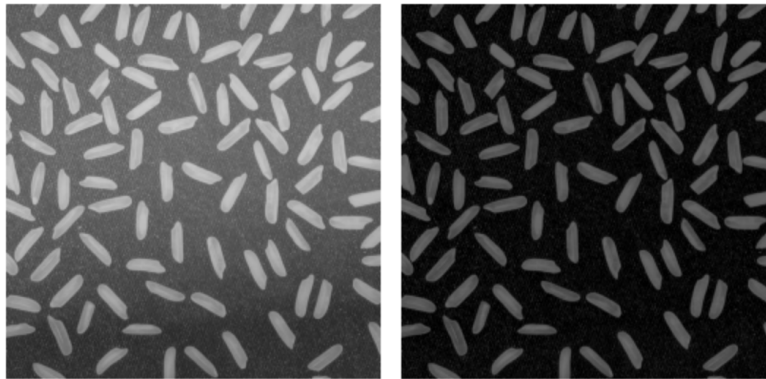


Figure 2.3: Original image (left) and image filtered with the tophat filter (right). Images reproduced with permission. ©1994-2021 The MathWorks, Inc. All rights reserved.

A median filter is used along with the morphology open filter to post-process the combined image after individual preprocessing of the stopping power and straggling power. The median filter takes a specified  $m \times n$  sized neighborhood around a corresponding pixel of the input image and replaces that pixel value with the median value

of the entire neighborhood. This filter technique is particularly useful for filtering out salt and pepper noise and smoothing images with less blurring than either a gaussian filter or averaging filter. The effect of applying a median filter on a greyscale image with salt and pepper noise is shown in Figure 2.4.



Figure 2.4: Image of coins with salt and pepper noise (left) and median filtered image (right). Image reproduced with permission. ©1994-2021 The MathWorks, Inc. All rights reserved.

### *Procedure and Results*

The base combined image generated by adding the stopping power and straggling power has a lot of introduced error from the reconstruction algorithm and uneven shading within elements of the phantom that are meant to be uniform. The initial combined image is displayed in Figure 2.5.



Figure 2.5: Combined proton image produced by adding stopping power and straggling power images.

In an effort to mitigate this error, different filtering techniques are applied to the individual stopping power and straggling power images and to the combined image. First, the morphology open filter is applied to the stopping power image in order to remove the error from the background and smooth out the phantom interior. This result alongside the unfiltered stopping power image is shown in Figure 2.6. Figures 2.7 and 2.8 show zoomed in sections of the phantoms in 2.6 to better display the differences. Figure 2.7 is an interior section of the phantom and 2.8 includes the phantom background.



Figure 2.6: Original stopping power image (left) and the image with open filter applied (right).

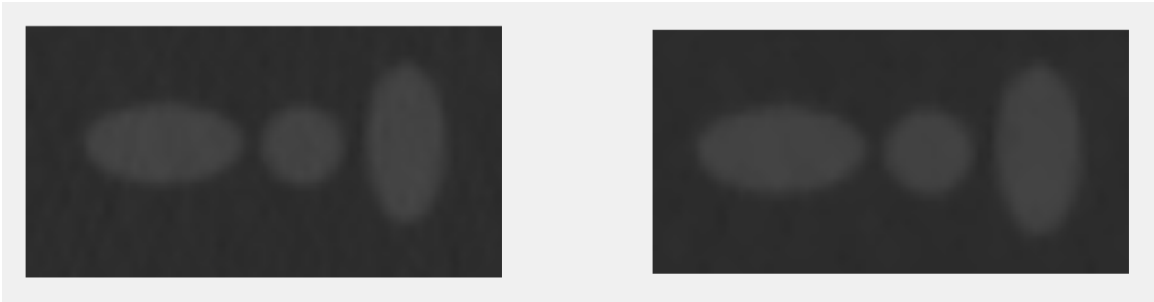


Figure 2.7: Zoomed in interior section of the original stopping power image (left) and the zoomed in interior section of the image with open filter applied (right).

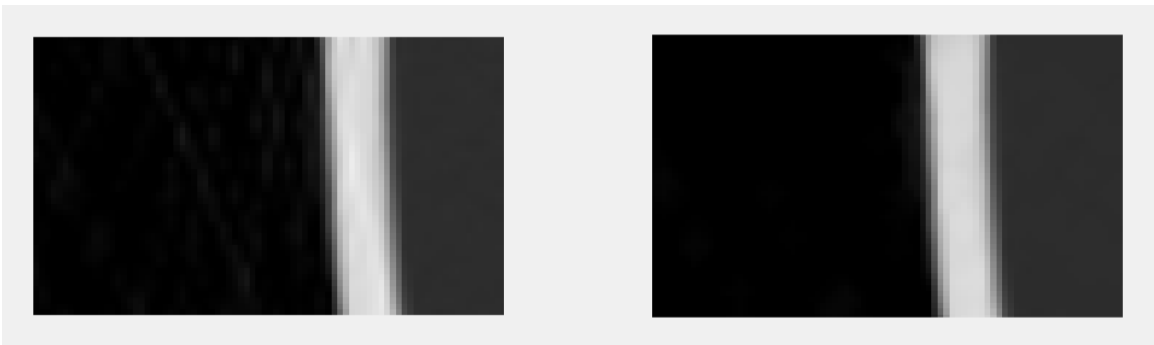


Figure 2.8: Zoomed in exterior section of the original stopping power image (left) and the zoomed in exterior section of the image with open filter applied (right)

The open filter does a satisfactory job in removing the thin white lines in the background and smooths the interior of the phantom substantially.

The straggling power image also has error present in the background, but the same filtering technique would not be beneficial since it would remove the desirable information. Because of this, the morphology tophat filter is applied. These results are shown in Figure 2.9 on the right, alongside the unfiltered straggling power image on the left.

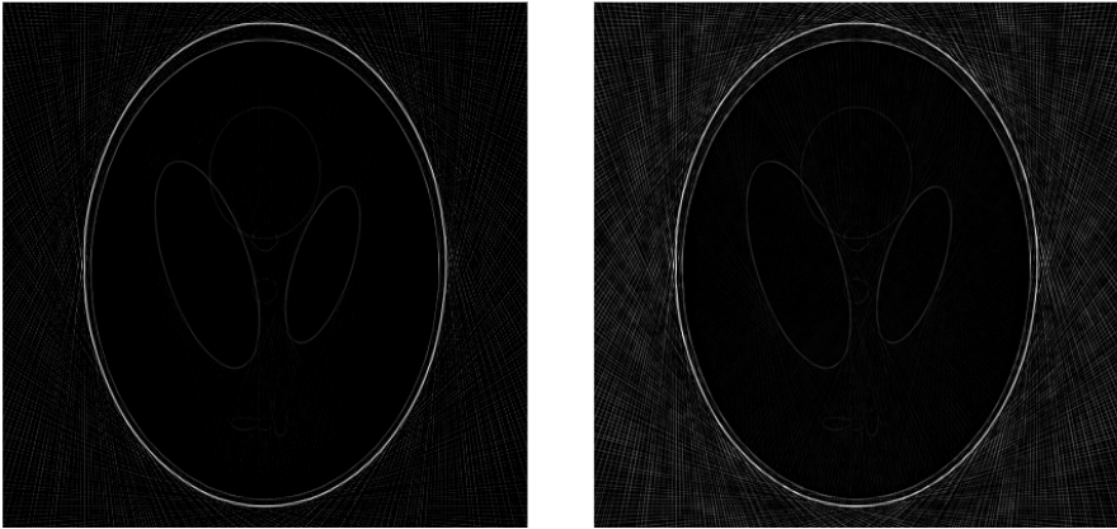


Figure 2.9: Original straggling power image (left) and the image with tophat filter applied (right).

This filter increased the background error as determined by inspection, which does not appear to be beneficial by comparing this filtered image to the unfiltered straggling power image. However, the tophat filter shifts the error, resulting in less constructive interference internal to the phantom and therefore less apparent error when combined with the filtered stopping power image. The new combined image adding the filtered stopping power and straggling power images is shown in Figure 2.10.



Figure 2.10. The new combined image with the filtered stopping and straggling power.

The variation in brightness within the phantom interior is more uniform in this new combined image, however the background of the phantom has more error than the initial combined image without the preprocessing filters. To remove this error, a for loop is added to the code that forces the pixels of the combined image to be black wherever the pixels of the stopping power image are black. The result of this addition is displayed in Figure 2.11.



Figure 2.11: Combined image forcing pixels to be black where corresponding stopping power pixels are black.

By inspection, the new combined image has significantly less error, but there is still some improvement that can be made. The open filter is applied again to shrink the bright error spots, and then a  $3 \times 3$  median filter is used to smooth the entirety of the image. This final result is shown in Figure 2.12.

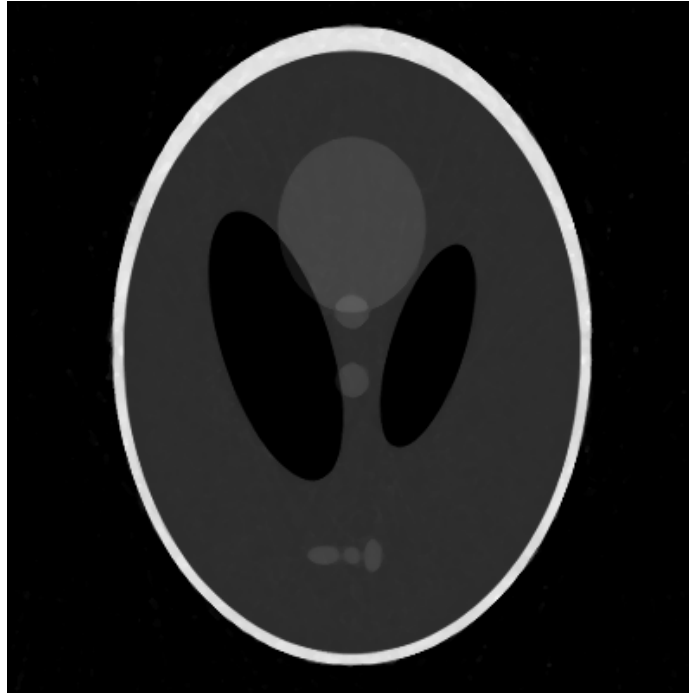


Figure 2.12. Final combined image after application of open filter and median filter.

This final image has removed nearly all the error introduced by the reconstruction process. Figure 2.13 shows the initial combined image alongside the final filtered combined image for comparison. The filtered combined image shows significant smoothing of the image, however the interior artifacts of the phantom with less contrast appear to have a significant loss in precision.



Figure 2.13: Final combined image (left) compared to the original stopping power image (right).

#### *Discussion*

By visual inspection of Figure 2.13, much of the error that was present in the background of the original combined image is successfully removed. This allows for sharper edges along the boundaries of the phantom where high contrast is present, but the boundaries of internal artifacts with less contrast are less precise. Considering the importance of precision along the boundaries of the internal artifacts, this filtering technique was not beneficial for the desired result of sharpening all of the artifact boundaries within the image.

## CHAPTER THREE

### Applying Knowledge of Straggling Power Data to Adjust Image

#### *Introduction*

Applying normal image processing techniques such as filtering to the stopping power, straggling power, and combined image was not beneficial to sharpening the edges of the combined stopping power and straggling power pCT image. A  $4000 \times 4000$  bit original phantom with stopping/straggling section size of  $20 \times 20$  bits was used for further experimentation. These sizes were chosen in order to get better statistics for the stopping power and straggling power. Since straggling power contains significantly less information than stopping power, a weight of 0.4 was put on the straggling power during its addition with the stopping power in order to reduce the size of the spikes on the combined image. A mask is also generated and applied to the straggling power to remove the noise from the background of the straggling power phantom. The new combined image created with the modified straggling power is then filtered with a  $3 \times 3$  median filter to smooth the data. These modifications result in significantly steeper slopes along the edges as viewed on a RSP vs. depth in cm line graph. These results are then tested for robustness by applying the techniques to combined images created with different original phantom sizes and stopping/straggling section sizes. The results from the robustness testing show that the improvement in the edge slope is proportional to the ratio of the stopping/straggling section size and the original phantom size. Quantitative analysis is conducted on the data by calculating the FWHM for the stopping power, combined data, and original phantom and corroborated the qualitative results that the combined image does improve the edge slope.

## *Background*

### *Masking*

Masking is a practice that is commonly used in medical imaging to clean up the background of an image. To create a mask, the area of interest is determined; any bits inside of this boundary are forced to 1 in the mask while bits outside of the boundary are forced to 0. This mask is then bit-wise multiplied with the image, removing any noise from the background. Implementing this in MATLAB requires a nested for loop to find the column where the data of interest begins and ends for each row. The area between the start and end of the data of interest is set to 1 while the rest of the mask is set to zero.

### *Full Width at Half Maximum*

FWHM is a statistic that is commonly calculated within medical imaging to quantify improvements. The FWHM is calculated for a single area of interest within an image by first measuring the maximum intensity. The width of the area is then calculated by counting all of the pixels that are at least half of the maximum intensity. The FWHM is used to help quantify the improvements on the image edges for this experiment.

## *Procedure and Results*

As shown in Chapter 2, applying traditional filtering techniques to the stopping and straggling power data as well as the combined image did not provide the desired effect of sharpening the edges of the phantoms, so a different approach was needed. A phantom image size of  $4000 \times 4000$  bits and stopping/straggling section size of  $20 \times 20$  bits is used for this testing.

Since the straggling power does not contain as much information about the phantom structures as the stopping power, the weight applied to the straggling power

during addition with the stopping power is reduced from 1 to 0.4. The value 0.4 is determined heuristically by examining the variation of the straggling power edge spike heights for beams traveling left to right versus right to left through the object (i.e. a 180 degree difference). See for example in Figure 3.1 the difference in the blue spikes just exterior to the "bone" portion of the image, where the straggling effect is greatest, at approximately 4 cm and 22 cm depth. The intensities of these spikes are approximately 1 and 0.6 respectively but should be equivalent, so the difference of the two values, 0.4, is chosen as the weight. Figures 3.1 and 3.2 show line graphs of relative stopping power (RSP) vs. depth in cm for a single row of phantom data taken from the center of the phantom. Figure 3.3 displays the location of the data taken for the line graphs as a red line on the original phantom. The total phantom width is assumed to be 20 cm. The 50th percentile for male's head breadth is 15.2 cm, and the head portion of the image is approximately 76% of the image width at the widest point [21]. This results in a total width of approximately 18.8 cm, which is rounded up to 20 cm for calculation simplicity. Figure 3.1 shows the stopping power, straggling power, and combined data for the straggling power weight of 1, and Figure 3.2 shows the same information for the straggling power weight of 0.4.

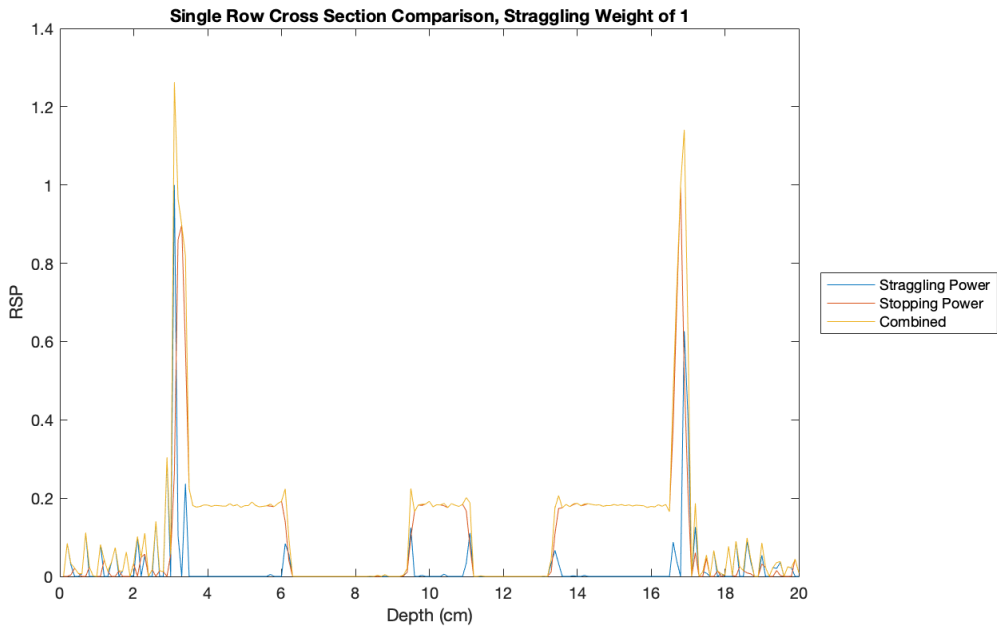


Figure 3.1: RSP vs. depth in cm line graphs of stopping power, straggling power, and combined with a straggling power weight of 1.

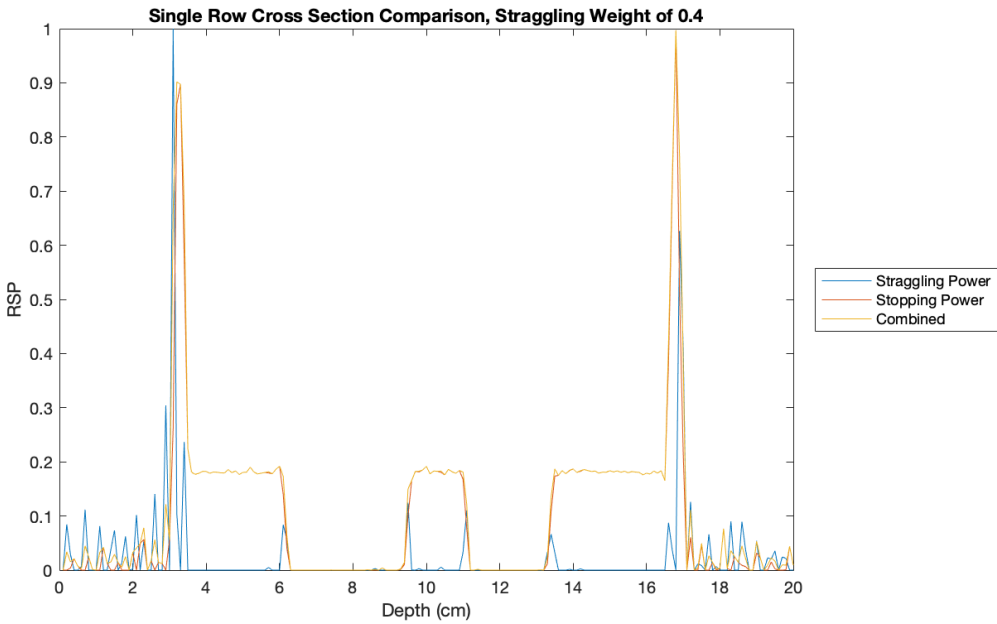


Figure 3.2: RSP vs. depth in cm line graphs of stopping power, straggling power, and combined with a straggling power weight of 0.4.



Figure 3.3. Position of data taken for line graphs on original phantom.

When the straggling power weight is 1, it creates large spikes in the combined image and pushes the maximum RSP well over the expected maximum of 1. By reducing the weight of the straggling power to 0.4, the larger straggling power spikes are able to increase the slope of the edges but the overshoot is reduced. The RSP is also kept at or below the desired maximum of 1. From these graphs, it is evident that the majority of noise is present outside of the phantom image and is caused primarily by the straggling power. To remove this error in the background of the straggling power, a mask is generated based off of the stopping power data. This mask consists of zeros in the background and ones internal to the phantom area; it is multiplied element-wise with the straggling power to remove all error from the background while keeping the phantom interior data. Figure 3.4 shows an example phantom mask and Figure 3.5 shows the resulting line graph of the mask being applied to the straggling power.

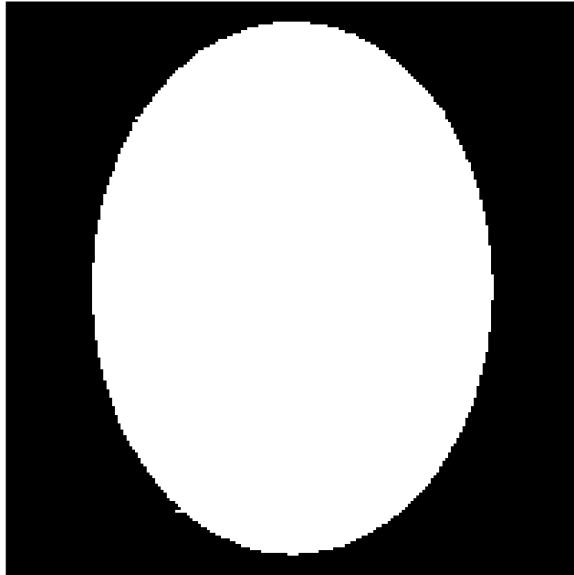


Figure 3.4. Generated phantom mask.

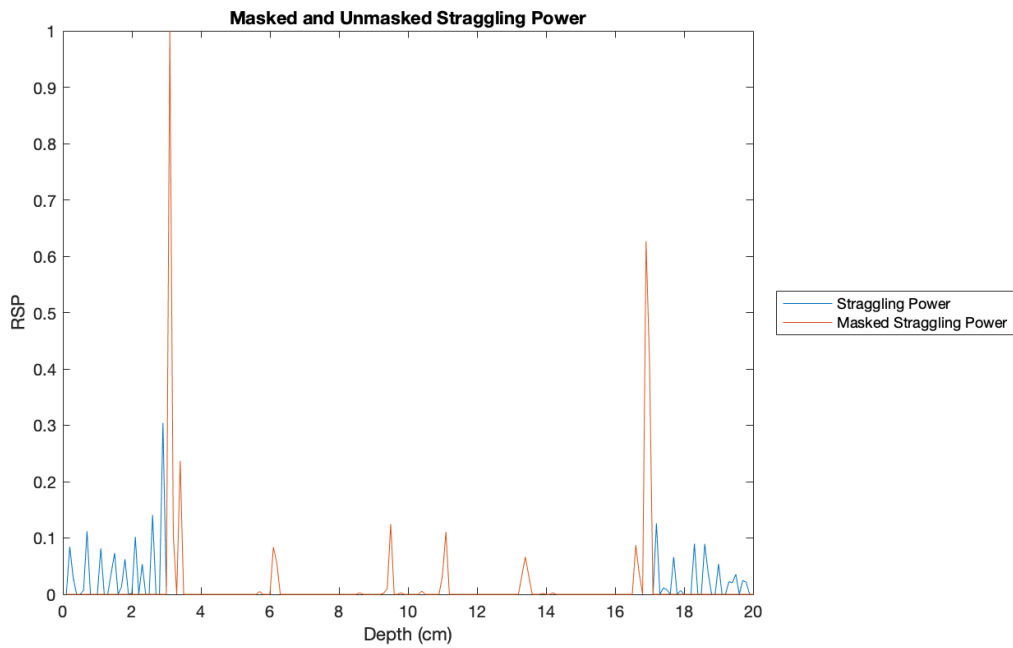


Figure 3.5. Straggling power with and without mask applied.

Applying the mask to the straggling power successfully removes nearly all error from the background of the straggling power image while leaving the phantom interior intact. From this graph, it is evident that the addition of the modified straggling power

with the stopping power will still result in some sharp peaks, and the image will still have some error present from the stopping power. A  $3 \times 3$  median filter is applied to the new combined data to smooth the noise and peaks. This result is shown in Figure 3.6.

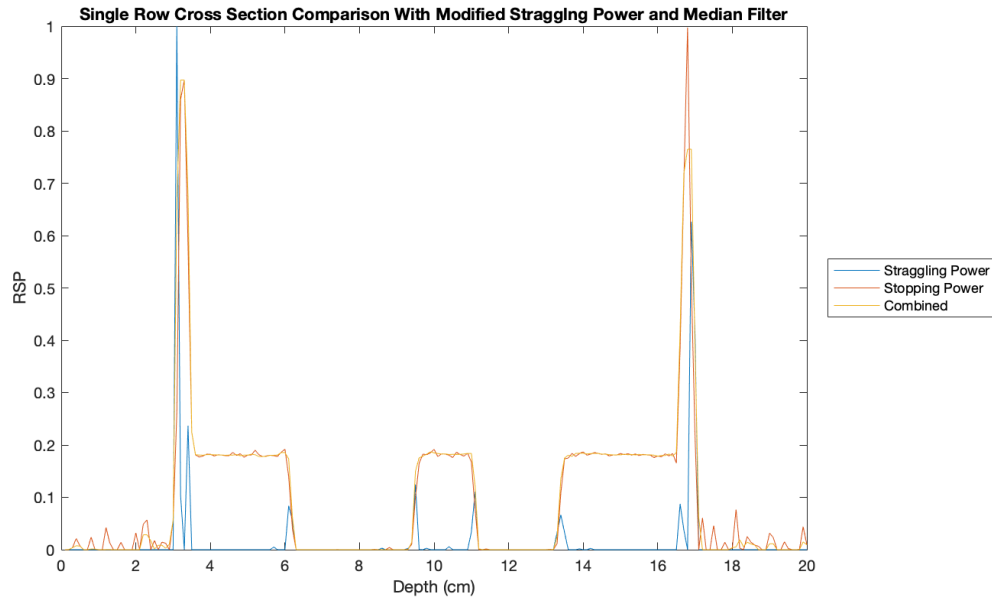


Figure 3.6. Line graph cross section with masked and weighted straggling power.

By weighting and applying the mask to the straggling power along with applying the median filter, the new combined image is much cleaner than before. By inspection, the slope of the data along the phantom artifact boundaries is significantly steeper. Zooming into the graph displays this more clearly as shown in Figure 3.7.

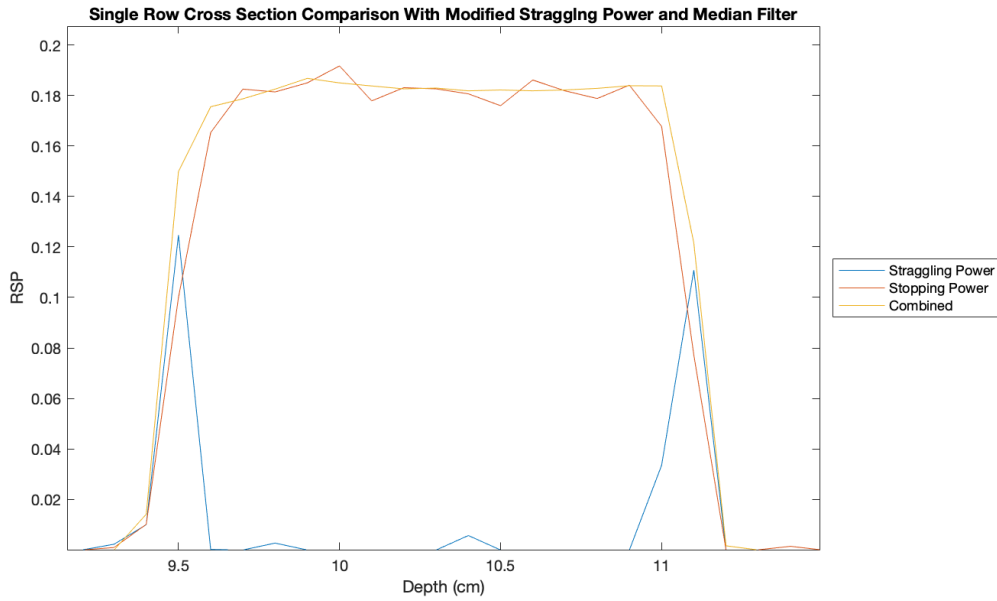


Figure 3.7. Zoomed in cross section of modified combined image.

The steepness of the slope translates to the sharpness of the edge in the picture. The new combined image with weighted and masked straggling power shows significant improvement of these slopes. These techniques are then applied to images of different sizes to check for robustness for potential differences in equipment.

Phantom images of various larger sizes and different stopping/straggling section sizes are tested to see if the results hold for different image sizes. Due to the size of these images, the code is run on Baylor’s research facility compute nodes. Figures 3.8 and 3.9 show the full line graph and zoomed in cross section of the stopping power, straggling power, and combined image for an original phantom size of  $16000 \times 16000$  bits with  $50 \times 50$  bit stopping and straggling power sections. This results in stopping and straggling power images of size  $320 \times 320$  bits.

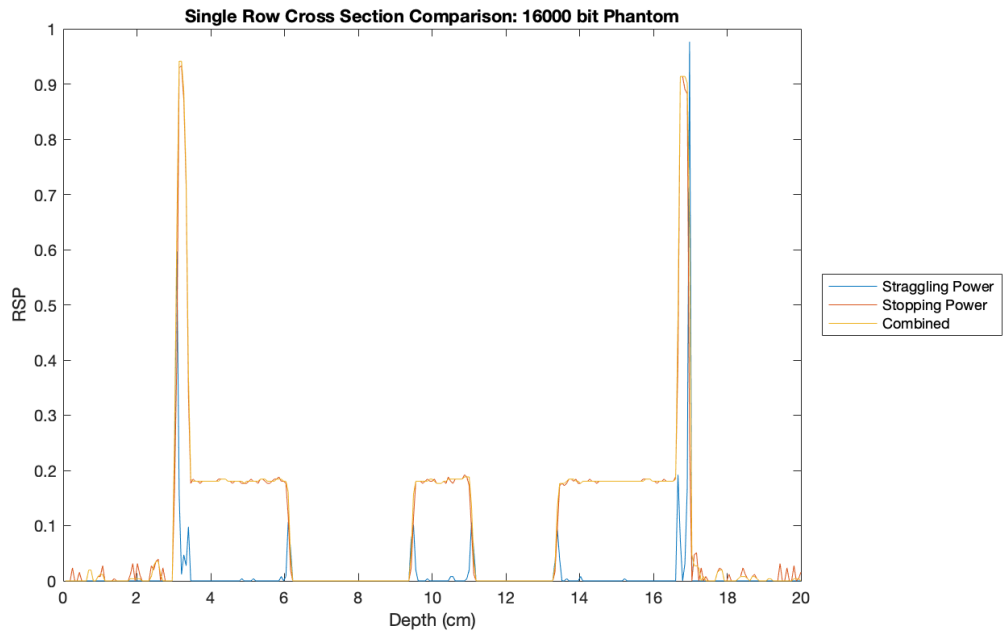


Figure 3.8: Line graph cross section with masked and weighted stragglng power for phantom size  $16000 \times 16000$  bits and stopping/stragglng sections of  $50 \times 50$  bits.

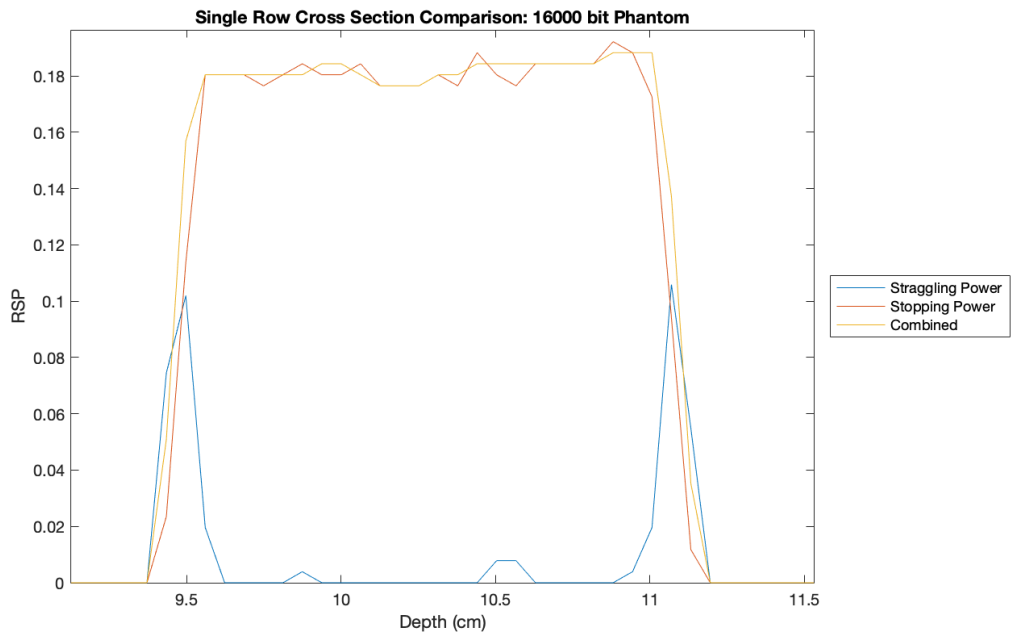


Figure 3.9: Zoomed in cross section for phantom size  $16000 \times 16000$  bits and stopping/s-tragglng sections of  $50 \times 50$  bits.

These results are very similar to that of the  $4000 \times 4000$  bit phantom with  $20 \times 20$  bit stopping/straggling section size. Figures 3.10 and 3.11 show the results for a phantom size of  $32000 \times 32000$  bits with stopping/straggling sections of  $50 \times 50$  bits, resulting in stopping/straggling power images of size  $640 \times 640$ .

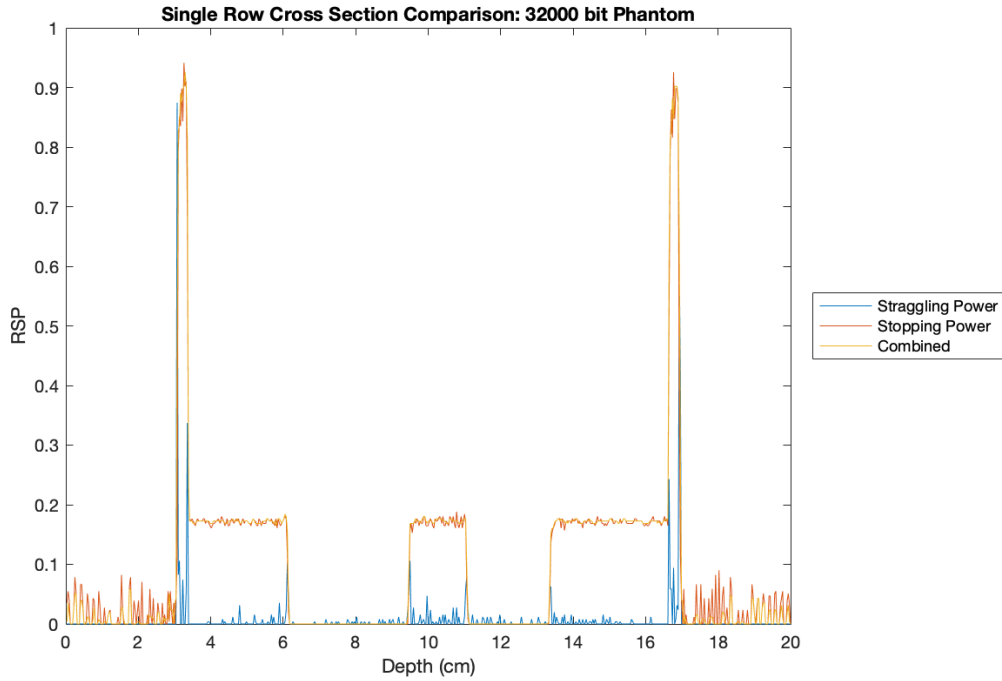


Figure 3.10: Line graph cross section with masked and weighted straggling power for phantom size  $32000 \times 32000$  bits and stopping/straggling sections of  $50 \times 50$  bits.

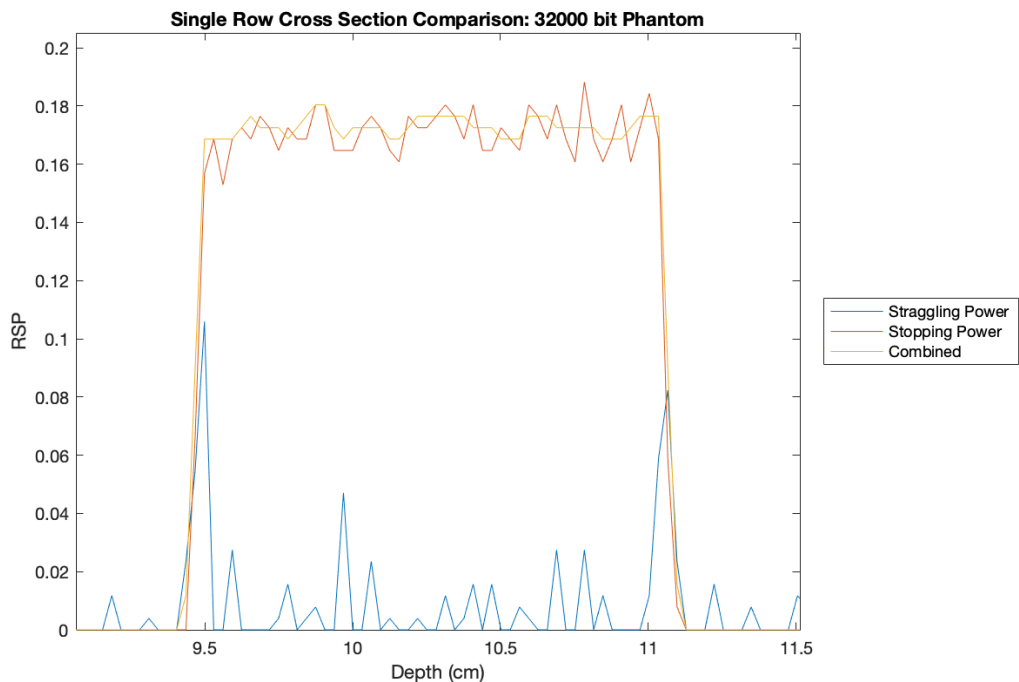


Figure 3.11: Zoomed in cross section for phantom size  $32000 \times 32000$  bits and stopping/s-tragging sections of  $50 \times 50$  bits.

The slope improvement with this data is much less substantial than the previous two. This is due to the smaller ratio of the stopping/s-tragging section size to original phantom size. Since this ratio is smaller, the stopping power is a more accurate approximation of the original phantom than the previous examples. However, there still is a small slope improvement along the edges due to the addition of the stragging power. Figures 3.12 and 3.13 show the results for a phantom size of  $64000 \times 64000$  bits with stopping/s-tragging sections of  $200 \times 200$  bits, resulting in stopping/s-tragging power images of size  $320 \times 320$ .

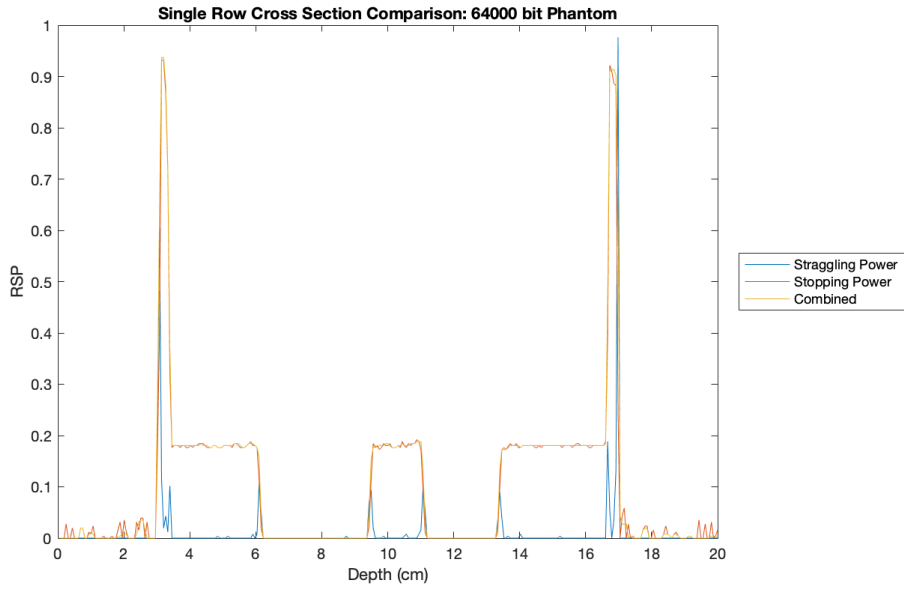


Figure 3.12: Line graph cross section with masked and weighted stragglng power for phantom size  $64000 \times 64000$  bits and stopping/stragglng sections of  $200 \times 200$  bits.

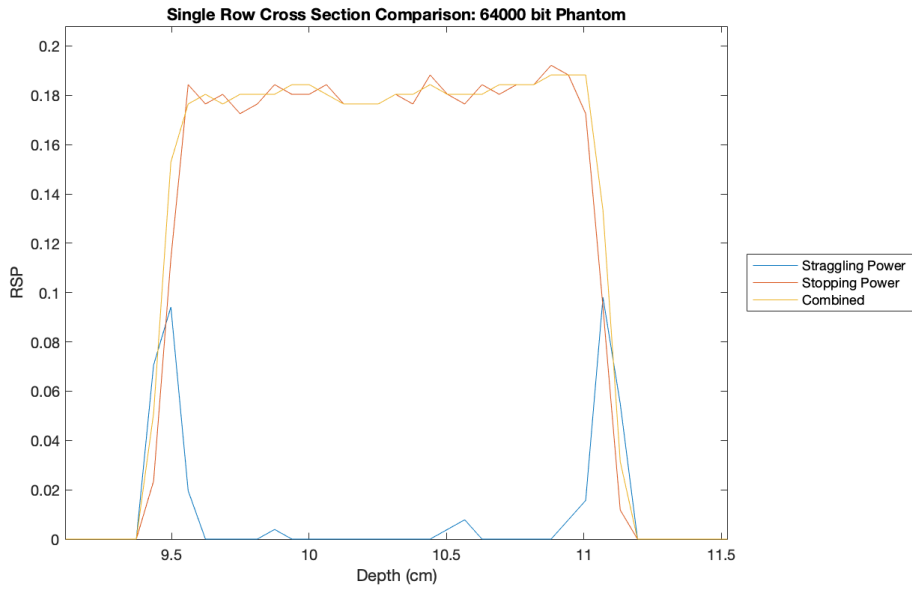


Figure 3.13: Zoomed in cross section for phantom size  $64000 \times 64000$  bits and stopping/s-tragglng sections of  $200 \times 200$  bits.

These results are nearly identical to those of the  $16000 \times 16000$  bit phantom with  $50 \times 50$  bit stopping/stragglng section size since the ratio of section size to

phantom size is the same. This result displays that the edge improvement from the addition of the straggling power is proportional to the size of the ratio between the section size and original phantom size.

### *Quantitative Analysis*

To show the edge improvement quantitatively, the FWHM measurement is taken for the stopping power and straggling power along the same center anomaly displayed in the zoomed in images above. These values are shown in Table 3.1.

Table 3.1. FWHM values for stopping power image and combined image for different phantom and section sizes.

Phantom Size [bits]	Detector Size [bits]	Number of Pixels (phantom/detector)	Pixel Size [mm]	Stopping Power FWHM [mm]	Combined Power FWHM [mm]	Actual FWHM [mm]	Stopping Power Error [mm]	Combined Error [mm]	Improvement [mm]
4000	20	200	1	15.84	16.64	16.63	-0.79	0.01	0.78
16000	20	800	0.25	15.84	16.03	16.63	-0.79	-0.6	0.19
16000	50	320	0.625	15.84	16.37	16.63	-0.79	-0.26	0.53
32000	50	640	0.3125	15.79	15.99	16.63	-0.84	-0.64	0.2
64000	100	640	0.3125	15.79	15.98	16.63	-0.84	-0.65	0.19
64000	200	320	0.625	15.84	16.33	16.63	-0.79	-0.3	0.49
<b>Average Improvement [mm]:</b>									<b>0.3967</b>

For each variation, the combined image has a larger FWHM. The maximum calculated improvement is 0.78 mm, the minimum improvement is 0.19 mm, and the average calculated improvement is 0.3967 mm. It should be noted that the reference phantom FWHM for the same area is 21.35 mm; this value was measured for the highest resolution phantom and used for every comparison.

### *Discussion*

Incorporating a smaller straggling power weight, a masked on the straggling power, and a median filter on the combined image, the final combined image shows an improvement upon the steepness of the edge slopes. Experimenting with different original phantom and stopping/straggling section sizes showed that this improvement is proportional to the ratio between the section size and original phantom size. The slope improvement is analyzed quantitatively by calculating the FWHM for the center anomaly for the stopping power, combined image, and original phantom. These findings corroborate those of qualitative analysis, showing that the combined stopping power and straggling power do provide a significant improvement on edge slopes. Given the application for use in cancer treatment, even a small amount of improvement is substantial. Doctors are wanting to target small areas such as hematomas or tumors within the human body, and a millimeter of error could be the difference between destroying the targeted damaged tissue and the healthy tissue.

## CHAPTER FOUR

### Conclusion

Proton therapy utilizing radiography and computed tomography has been proven to be a viable alternative to X-ray radiography and CT scans. Four different types of data are collected during a pCT scan: stopping power, scattering power, fluence, and straggling power. Historically, image reconstructions have only utilized either stopping power or scattering power which both provide a decent overall image, but do not have sharp precision along artifact edges. For this study, it was proposed that combining the straggling power, which produces reconstructed images consisting of sharp artifact boundaries, with stopping power could produce a sharper overall image. This theory was first tested by simulating the stopping power and straggling power on MATLAB and adding the information to create a combined image. This resulted in an image with lots of introduced noise due to the constructive interference of error introduced by the reconstruction algorithm. There was also a lot of intensity variation within the combined phantom image where the brightness should have been uniform. In an effort to mitigate the error, typical filtering techniques were applied. The individual stopping and straggling power images were preprocessed with a morphology open filter and tophat filter respectively, and then the new combined image was post-processed with another morphology open filter and a  $3 \times 3$  median filter. This resulted in an image that did have significantly reduced error, however it was not beneficial for the purpose of sharpening the edges of the phantom's interior artifacts. Another experiment was conducted utilizing different techniques. It was noted that the straggling power contains significantly less information about the structure of the phantom compared to the stopping power, so the weight on the straggling power was reduced from 1 to 0.4 when added with the stopping power, resulting in

less severe spiking in the combined image. It was also determined that the stopping power data contained a lot of noise in the area exterior to the phantom, so a mask was generated based off of the important information within the stopping power data and then applied to the straggling power. This wiped out nearly all noise external to the phantom in the straggling power. With these two modifications, the combined image was already presenting a significant slope improvement along the artifact edges, but there was still a fair amount of noise and spiking present in the data. A  $3 \times 3$  median filter was applied to help smooth the data, resulting in a much cleaner image. These results were then tested for robustness by applying the process to original phantoms of various sizes and stopping/straggling sections of different sizes. It was shown that the slope improvement was proportional to the ratio between the section size and original phantom size. To show these results quantitatively, the FWHM was taken for the center anomaly of the cross-section data for the stopping power, combined image, and original phantom. The FWHM values showed that using the combined data has an average width improvement of 0.3967 mm compared to the stopping power, corroborating the results of visual inspection that the edge slope is significantly improved.

When compared to the unaltered stopping power, which is used for most pCT image reconstructions, the new combined images showed a notable slope improvement along the artifact boundaries. This improvement is vital for practical medical use since the aim of proton therapy is to target and destroy damaged tissue, and the difference between hitting the targeted area and harming healthy tissue can be a fraction of a millimeter. The improvement of edge sharpness displayed in this experiment, even at its least significant, would greatly improve the accuracy of proton therapy. Further research will still need to be conducted to verify the viability of this technique; only simulated data was able to be tested thus far, so the procedure will need to be tested on real data to verify the slope improvement.

## APPENDICES

## APPENDIX A

### Code Appendix

Listing A.1: MatLab code for creating stopping and straggling power images and modifying for the final combined output.

---

```
clear all
close all

%% Create base Phantom image
sz = 64000;
[P, E] = phantom('Modified_Shepp-Logan',sz);

%% Take Radon
R = radon(P, [0:359]);
[m,n] = size(R);

s = 200; % Size of sections for straggling and stopping power approximations

% Comparison phantom that is the same size as approximations:
P_comp = phantom('Modified_Shepp-Logan', sz/s);

%% Create stopping power and scattering power approximations
for i = 1:n
    for j = s:s:m
        if j == s
            b_stop(1,i) = mean(R(1:s, i));
            b_strag(1,i) = std(R(1:s, i));
        else
            b_stop(j/s, i) = mean(R(j-(s-1):j, i));
            b_strag(j/s, i) = std(R(j-(s-1):j, i));
        end
    end
end

%% Reconstruct the approximations and normalize
I_stop = FBP(b_stop, 0:359);
```

```

I_stop = I_stop / max(max(I_stop));

I_strag = FBP(b_strag, 0:359);
I_strag = I_strag / max(max(I_strag));

[m,n] = size(I_stop);

for i = 1:m
    for j = 1:n

        if (I_stop(i,j) < 0)
            I_stop(i,j) = 0;
        else
            I_stop(i,j) = I_stop(i,j);
        end

        if (I_strag(i,j) < 0)
            I_strag(i,j) = 0;
        else
            I_strag(i,j) = I_strag(i,j);
        end
    end
end

%% Adjust individual images to remove error in desired area
%se1 = strel('disk', 1);
%se2 = strel('disk', 2);
%I_stop = imopen(I_stop, se1);

%% Remove noise on outside of stragglng power
I_mask = zeros(m,n);
mask_start = -1;
mask_end = -1;

for i = 1:m
    mask_start = -1;
    for j = 1:n
        if (I_stop(i,j) > 0.1) && (mask_start < 0)
            mask_start = j;
        end
        if I_stop(i,j) > 0.1

```

```

        mask_end = j;
    end
end
if mask_start > 0
    I_mask(i, mask_start:mask_end) = 1;
end
end

I_strag = I_mask .* I_strag;

%% Add stopping and straggling power images
I_add = (I_stop + 0.4 * I_strag);

%% Filter out thin white error and smooth

I_add = medfilt2(I_add, [3 3]);

%% Figures
image_orig_name = sprintf('og_phantom_%d_%d.png', sz, s);
imwrite(P_comp, image_orig_name);

image_stop_name = sprintf('stop_phantom_%d_%d.png', sz, s);
imwrite(I_stop, image_stop_name);

image_strag_name = sprintf('strag_phantom_%d_%d.png', sz, s);
imwrite(I_strag, image_strag_name);

image_comb_name = sprintf('comb_phantom_%d_%d.png', sz, s);
imwrite(I_add, image_comb_name);

```

---

Listing A.2. MatLab code for creating the FBP reconstruction algorithm.

---

```

function I = FBP(sino, theta)

    [proj, angles] = size(sino);
    n = 2 * floor(proj / (2*sqrt(2)));
    pad = 2^(ceil(log2(proj)) + 1) - proj;
    step = 2 / (proj + pad);

    % Pad image with zeros

```

```

if pad > 0
    sino = [sino
            zeros(pad, angles)];
else
    sino = sino;
end

if min(size(theta)) == 1
    if angles == max(size(theta))
        I = zeros(n,n);

        % Make filter - ramp
        filter=[0:step:1 1-step:-step:step]';

        % Do fbp for each angle
        for angle = 1:angles

            % Filter
            fsino = real(ifft(fft(sino(:,angle)) .* filter));
            filtsino = fsino(1:proj);

            % Backproject
            T = imrotate(filtsino * ones(1,2*n), theta(angle)+90, 'bilinear');

            % Sum up just part in image
            [tr,tc] = size(T);
            startr = ceil((tr - n) / 2) + 1;
            startc = ceil((tc - n) / 2) + 1;
            Temp = T(startr:startr + n-1, startc:startc + n-1);
            I = I + Temp;
        end

        I = I * pi / (2*angles);
    else
        I = [];
    end
end
end

```

---

## REFERENCES

- [1] W. Commons, "File:braggpeak.png — wikimedia commons, the free media repository," 2020, [Online; accessed 14-April-2021]. [Online]. Available: <https://commons.wikimedia.org/w/index.php?title=File:BraggPeak.png&oldid=488534765>
- [2] G. Poludniowski, N. M. Allinson, and P. M. Evans, "Proton radiography and tomography with application to proton therapy," *The British Journal of Radiology*, vol. 88, p. 20150134, Jun 2015. [Online]. Available: <https://doi.org/10.1259/bjr.20150134>
- [3] H. Paganetti, "Range uncertainties in proton therapy and the role of Monte Carlo simulations," *Physics in Medicine and Biology*, vol. 57, no. 11, pp. R99—R117, May 2012.
- [4] K. M. Hanson, J. N. Bradbury, R. A. Koeppe, R. J. Macek, D. R. Machen, R. Morgado, M. A. Paciotti, S. A. Sandford, and V. W. Steward, "Proton computed tomography of human specimens," *Physics in Medicine and Biology*, vol. 27, no. 1, pp. 25–36, Jan 1982. [Online]. Available: <https://doi.org/10.1088/0031-9155/27/1/003>
- [5] C.-A. C. Fekete, P. Doolan, M. F. Dias, L. Beaulieu, and J. Seco, "Developing a phenomenological model of the proton trajectory within a heterogeneous medium required for proton imaging," *Physics in Medicine and Biology*, vol. 60, no. 13, pp. 5071–5082, 2015. [Online]. Available: <http://stacks.iop.org/0031-9155/60/i=13/a=5071>
- [6] R. I. MacKay, "Image guidance for proton therapy," *Clin. Oncol. (R. Coll. Radiol.)*, vol. 30, no. 5, pp. 293–298, 2018. [Online]. Available: <http://iopscience.iop.org/article/10.1088/1361-6633/aa8b1d/meta>
- [7] G. Cuttone, G. Cirrone, G. Candiano, F. D. Rosa, G. Russo, N. Randazzo, V. Sipala, S. L. Nigro, D. L. Presti, J. Feldt, J. Heimann, H. F.-W. Sadrozinski, A. Seiden, D. Williams, V. A. Bashkirov, R. W. Schulte, M. Bruzzi, and D. Menichelli, "Monte Carlo studies of a proton computed tomography system," *IEEE Transactions on Nuclear Science*, vol. 54, pp. 1487–1491, Oct 2007.

- [8] M. Bruzzi, N. Blumenkrantz, J. Feldt, J. Heimann, H. F.-W. Sadrozinski, A. Seiden, D. Williams, V. A. Bashkirov, R. W. Schulte, D. Menichelli, M. Scaringella, G. Cirrone, G. Cuttone, N. Randazzo, V. Sipala, and D. L. Presti, “Prototype tracking studies for proton CT,” *IEEE Transactions on Nuclear Science*, vol. 54, pp. 140–145, Feb 2007.
- [9] Y. Chen, E. Gomez, R. F. Hurley, Y. Nie, K. E. Schubert, and R. W. Schulte, “Accurate proton beam localization,” in *Proceedings of The 2012 International Conference on Bioinformatics and Computational Biology (BIOCOMP’12)*, 2012, pp. 213–217.
- [10] R. P. Johnson, “Review of medical radiography and tomography with proton beams,” *Reports on Progress in Physics*, vol. 81, no. 1, p. 016701, 2018. [Online]. Available: <http://stacks.iop.org/0034-4885/81/i=1/a=016701>
- [11] N. Matsufuji, H. Tomura, Y. Futami, H. Yamashita, A. Higashi, S. Minohara, M. Endo, and T. Kanai, “Relationship between CT number and electron density, scatter angle and nuclear reaction for hadron-therapy treatment planning,” *Physics in Medicine and Biology*, vol. 43, pp. 3261—3275, 1998.
- [12] M. Scaringella, M. Bruzzi, M. Bucciolini, M. Carpinelli, G. A. P. Cirrone, C. Civinini, G. Cuttone, D. L. Presti, S. Pallotta, C. Pugliatti, N. Randazzo, F. Romano, V. Sipala, C. Stancampiano, C. Talamonti, E. Vanzi, and M. Zani, “A proton computed tomography based medical imaging system,” *Journal of Instrumentation*, vol. 9, no. 12, p. C12009, 2014. [Online]. Available: <http://stacks.iop.org/1748-0221/9/i=12/a=C12009>
- [13] H. Fuchs, S. Vatnitsky, M. Stock, D. Georg, and L. Grevillot, “Evaluation of gate/geant4 multiple coulomb scattering algorithms for a 160mev proton beam,” *Nuclear Instruments and Methods in Physics Research Section B: Beam Interactions with Materials and Atoms*, vol. 410, pp. 122–126, 2017. [Online]. Available: <https://www.sciencedirect.com/science/article/pii/S0168583X17307826>
- [14] S. N. Penfold and Y. Censor, “Techniques in iterative proton CT image reconstruction,” *Sensing and Imaging*, vol. 16, no. 1, Oct 2015. [Online]. Available: <https://doi.org/10.1007/s11220-015-0122-3>
- [15] B. Schaffner and E. Pedroni, “The precision of proton range calculations in proton radiotherapy treatment planning: experimental verification of the relation between CT-HU and proton stopping power,” *Physics in Medicine and Biology*, vol. 43, pp. 1579–1592, 1998.

- [16] V. A. Bashkirov, R. W. Schulte, R. F. Hurley, R. P. Johnson, H. F.-W. Sadrozinski, A. Zatserklyaniy, T. Plautz, and V. Giacometti, “Novel scintillation detector design and performance for proton radiography and computed tomography,” *Medical Physics*, vol. 43, no. 2, pp. 664–674, 2016. [Online]. Available: <https://aapm.onlinelibrary.wiley.com/doi/abs/10.1118/1.4939255>
- [17] B. E. Schultze, P. Karbasi, V. Giacometti, T. E. Plautz, K. E. Schubert, and R. W. Schulte, “Reconstructing highly accurate relative stopping powers in proton computed tomography,” in *Proceedings of the IEEE Nuclear Science Symposium & Medical Imaging Conference (NSS/MIC) 2015*, Oct 2015, pp. 1–3.
- [18] G. Ramachandran and A. Lakshminarayanan, “Three dimensional reconstructions from radiographs and electron micrographs: Application of convolution instead of Fourier transforms,” *Proceedings of the National Academy of Sciences of the United States of America*, vol. 68, pp. 2236–2240, 1971.
- [19] L. Shepp and B. Logan, “The Fourier reconstruction of a head section,” *IEEE Transactions on Nuclear Science*, vol. NS-21, pp. 21–43, 1974.
- [20] K. Sreedhar and B. Panlal, “Enhancement of images using morphological transformation,” *CoRR*, vol. abs/1203.2514, 2012. [Online]. Available: <http://arxiv.org/abs/1203.2514>
- [21] J. W. Young, “Head and face anthropometry of adult u.s. civilians,” pp. 0–44, 1993. [Online]. Available: <https://apps.dtic.mil/dtic/tr/fulltext/u2/a268661.pdf>